Resonant energy transfer Rb ns + Rb ns + $2h\nu$ → Rb $np_{1/2}$ + Rb $np_{3/2}$ in a frozen Rydberg gas

J. Nunkaew,[1,*] Raheel Ali,[2,3] and T. F. Gallagher[3]

[1]*Thailand Center of Excellence in Physics, Ministry of Higher Education, Science, Research and Innovation, 328 Si Ayutthaya Road, Bangkok 10400, Thailand*

[2]*Quaid-i-Azam University, Islamabad 45320, Pakistan*

[3]*Department of Physics, University of Virginia, Charlottesville, Virginia 22904, USA*

(Received 8 June 2020; accepted 4 August 2020; published 28 August 2020)

We have observed the process Rb ns + Rb $ns + 2h\nu \rightarrow$ Rb $np_{1/2}$ + Rb $np_{3/2}$ from $n = 34$ to $n = 40$ in a frozen gas of Rb Rydberg atoms. It is resonant when the microwave frequency is halfway between the $ns \rightarrow np_{1/2}$ and $ns \rightarrow np_{3/2}$ frequencies, which range from 57 to 106 GHz. The process cannot occur in isolated atoms, nor can it occur if the magnetic quantum numbers are unchanged, an implicit assumption of one-dimensional models. A Floquet-Forster model shows that the coupling between the initial and final states involves the absorption of two microwave photons and the dipole-dipole interaction, which leads to a coupling proportional to the product of the density, the microwave field squared, and n^{*14}, where n^* is the effective quantum number of the $np_{3/2}$ state. We have experimentally verified these dependences. The observed resonances are asymmetric, with a low-frequency tail, which we attribute to the van der Waals shift of the final $np_{1/2}np_{3/2}$ state due to its dipole-dipole interaction with the nearby $ns(n + 1)s$ state. While the van der Waals shift is negligible for most of the atoms in the Rydberg gas, it is not for the pairs of close atoms which undergo this transition.

DOI: 10.1103/PhysRevA.102.023332

I. INTRODUCTION

Cold Rydberg atoms are of interest for quantum gates and simulators because of their large electric dipole moments, which scale as the square of the principal quantum number n [1–9]. In atomic units, which we use unless specified otherwise, the dipole-dipole interaction between a pair of Rydberg atoms is given approximately by $V_{dd} = n^4/R^3$, where R is the distance between the two atoms, and it is significant even when the atoms are micrometers apart. The combination of the long range of the dipole-dipole interaction and the sub-mK temperature of the cold atoms means that on a timescale of microseconds atoms at a density of $\sim 10^{10}$ cm^{-3} move a negligible fraction of their typical spacing. As a result, an assembly of cold Rydberg atoms is often termed a frozen Rydberg gas.

An example of the use of Rydberg atoms for quantum information is the use of the off-resonant dipole-dipole, or van der Waals, interaction to produce excitation blockades [9–12]. The van der Waals interaction is given approximately by $V_{vdW} = n^8/\Delta R^6$, where Δ is the energy spacing between the dipole-dipole coupled states. Over a limited range of n it is often the case that $\Delta \sim n^{-3}$, resulting in van der Waals interactions scaling as n^{11}. A second important example of the dipole-dipole interaction is Forster-resonant dipole-dipole energy transfer, potentially useful for simulations [13–16]. Forster resonances are often tuned into resonance using a static electric field. In many cases the requisite fields are small due to the large electric dipole moments of the Rydberg atoms and the near degeneracy of the dipole-dipole coupled states. In some cases, though, a small field tunes nearly degenerate levels away from the Forster resonance, and alternative methods must be employed. One is to use the AC Stark shift from a near resonant transition to tune the levels into resonance [17]. Another approach is to create a Forster resonance with microwave or radio-frequency (RF) fields by driving transitions which are allowed in pairs of atoms but not in isolated atoms [18–23]. Transitions in which pairs of atoms, molecules, or ions absorb photons have been observed in condensed-matter systems [24,25], which are analogous to frozen Rydberg gases. In such cases the interacting absorbers are close to each other, 1 to 10 nm apart, which compensates for dipole moments which are orders of magnitude smaller than those of Rydberg atoms. A related phenomenon in the gas phase is a radiatively assisted collision, in which a pair of atoms absorbs a photon while colliding [26,27].

While creating a Forster resonance with an RF field is photon absorption or emission by the interacting pair of atoms, it is usually described in the following way. An electric field, which may be a combination of static and RF fields, produces a Stark shift of the atomic levels. If an RF field is present the energies of the atomic levels are modulated, which leads to sidebands displaced in energy by multiples of the RF frequency. The sidebands, which can be above and below the bare energy, can be tuned to create Forster resonances. In short, the primary effect of the field is to shift the atomic energies, not to alter the atomic states. A complete, lucid treatment of this approach has been given by van Ditzhuijzen *et al.* [19]. In contrast, creating a Forster resonance with a microwave field can often be understood as a normally forbidden microwave transition which is allowed due to a dipole-dipole-induced admixture to either the initial or the final state. Despite the differences in how they may be described, both

*jn8h@virginia.edu

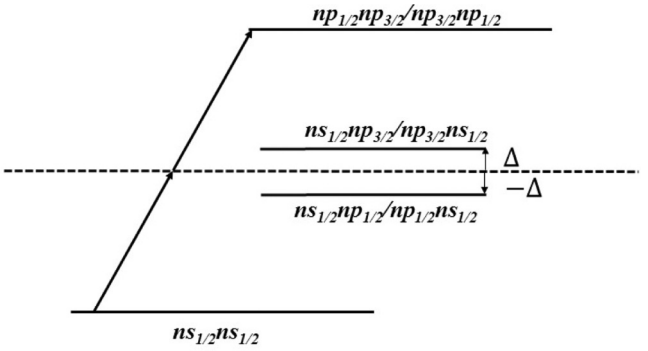

FIG. 1. Energy-level diagram for the two-photon microwave transition from the $ns_{1/2}ns_{1/2}$ state to the $np_{1/2}np_{3/2}$ and $np_{3/2}np_{1/2}$ states. The solid arrows represent the two microwave photons. The resonance frequency, midway between the atomic $ns_{1/2} - np_{1/2}$ and $ns_{1/2} - np_{3/2}$ frequencies, is detuned from the atomic transitions by $\pm\Delta$, half the fine-structure interval.

RF- and microwave-created Forster resonances are Forster resonances of Floquet states.

Here we describe an example of a Forster resonance enabled by a microwave transition. Specifically, we present a systematic study of the process [28]

$$\text{Rb } ns + \text{Rb } ns + 2\hbar\omega \rightarrow \text{Rb } np_{1/2} + \text{Rb } np_{3/2}, \qquad (1)$$

which is resonant at the microwave frequency midway between the $ns_{1/2} - np_{1/2}$ and $ns_{1/2} - np_{3/2}$ frequencies, as shown in Fig. 1. This process is very similar to that observed by Hettich *et al.*, who observed a transition midway between the absorption frequencies of two terrylene molecules 12 nm apart in a *para*-terphenyl crystal at 1.4 K [25]. The frequencies of the two molecules differ due to the difference in the local field environments. Essentially the same process as Eq. (1) was observed by Pedrozo-Penafiel *et al.* who observed laser excitation of Na atoms in a dense gas at the frequency midway between the Na $3s - 3p_{1/2}$ and $3s - 3p_{3/2}$ transition frequencies [29]. In this case the absorption occurred in the transient molecules formed during collisions; i.e., it is an example of a radiatively assisted collision [26]. Although the process of Eq. (1) appears to be simply a microwave transition, the most convenient way to describe it is as a Forster resonance of dressed, or Floquet, states [19,21,23,28].

There are several notable features of the process of Eq. (1) and Fig. 1. First, it is impossible to observe transitions at this frequency in isolated atoms or in a pair of noninteracting atoms. In the latter case the amplitudes via the two intermediate states cancel. Only when the dipole-dipole interaction in the intermediate states is present can the transition occur. Even then it is not allowed in what we might term a one-dimensional model, that is, one in which the m_j values, the azimuthal angular momentum quantum numbers, of the two atoms do not change in the transition. The full three-dimensional character of the the dipole-dipole interaction must be taken into account, resulting in a nonzero coupling between the initial and final states. Finally, the coupling in the process of Eq. (1) scales very rapidly with n, specifically as n^{*14}, where n^* is the effective quantum number of the $np_{3/2}$ state.

TABLE I. Floquet states and energies.

State	Energy
$ns_{1/2}ns_{1/2} + \omega$	$W_{ns_{1/21/2}} + \omega$
$ns_{1/2}np_{1/2}$	$W_{ns_{1/2}np_{1/2}}$
$np_{1/2}ns_{1/2}$	$W_{np_{1/2}ns_{1/2}}$
$ns_{1/2}np_{3/2}$	$W_{ns_{1/2}np_{3/2}}$
$np_{3/2}ns_{1/2}$	$W_{np_{3/2}ns_{1/2}}$
$np_{1/2}np_{3/2} - \omega$	$W_{np_{1/2}np_{1/2}} - \omega$
$np_{3/2}np_{1/2} - \omega$	$W_{np_{3/2}np_{1/2}} - \omega$

This paper is organized as follows. First we present a description of the process as a Forster resonance of Floquet levels to show the origin of the n^{*14} coupling. We then describe our experimental approach and present our observations. Finally, we compare our observations to expectations based on the Forster Floquet model and show that a van der Waals interaction is responsible for the asymmetric line shape.

II. FLOQUET DESCRIPTION

The microwave transition shown in Fig. 1 can be described as a Forster resonance of Floquet states, and we here use a one-dimensional model to provide a qualitative description of the process. The Floquet states are states of pairs of atoms with an integral number of microwave photons added or subtracted [30]. We consider the relevant, nearly degenerate Floquet states and Floquet energies given in Table I.

We can add an equal number of microwave photons to each state with no change in the calculated result, but the choice of Table I provides the most easily understood energy-level diagram, as shown by Fig. 2. We add one photon to the $ns_{1/2}ns_{1/2}$ state, which we denote $ns_{1/2}ns_{1/2} + \omega$, and we subtract one photon from the $np_{1/2}np_{3/2}$ and $np_{3/2}np_{1/2}$ states, which we denote $np_{1/2}np_{3/2} - \omega$ and $np_{3/2}np_{1/2} - \omega$. In Fig. 2 the broken lines show the

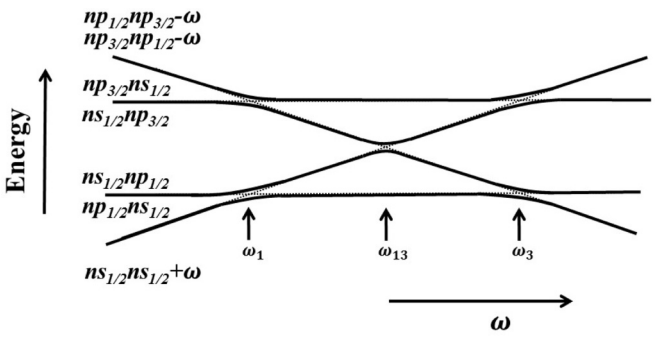

FIG. 2. Floquet energies for the molecular states of Fig. 1 vs microwave frequency. One microwave photon has been added to the $ns_{1/2}ns_{1/2}$ state and one has been subtracted from the $np_{1/2}np_{3/2}$ and $np_{3/2}np_{1/2}$ states. With the microwave field $E = 0$, shown by the broken lines, the levels cross at ω_1 and ω_3, the atomic resonance frequencies, and at ω_{13}, the resonance frequency for the $ns_{1/2}ns_{1/2} \rightarrow np_{1/2}np_{3/2}/np_{3/2}np_{1/2}$ transition. With $E \neq 0$, shown by the solid lines, there are large avoided crossings at ω_1 and ω_3. Adding the dipole-dipole interaction produces a small avoided crossing at ω_{13}. In the figure the avoided crossing at ω_{13} is exaggerated.

Floquet energies vs microwave frequency with a microwave field amplitude of $E = 0$. The Floquet energies of the $ns_{1/2}ns_{1/2} + \omega$ and $np_{1/2}np_{3/2} - \omega/np_{3/2}np_{1/2} - \omega$ states cross the $ns_{1/2}np_{1/2}/np_{1/2}ns_{1/2}$ and the $ns_{1/2}np_{3/2}/np_{3/2}ns_{1/2}$ states at the atomic $ns_{1/2} - np_{1/2}$ and $ns_{1/2} - np_{3/2}$ resonance frequencies ω_1 and ω_3. The $ns_{1/2}ns_{1/2} + \omega$ energy crosses the $np_{1/2}np_{3/2} - \omega/np_{3/2}np_{1/2} - \omega$ state at ω_{13}, the frequency of the $ns_{1/2}ns_{1/2} \rightarrow np_{1/2}np_{3/2}/np_{3/2}np_{1/2}$ transition. When the microwave field is nonzero the atomic $ns_{1/2} - np_j$ couplings lead to avoided crossings at ω_1 and ω_3, as shown by the solid lines of Fig. 2. The curvature of the energy levels indicates the degree of state mixing produced by the microwave field, and the nominal $ns_{1/2}ns_{1/2} + \omega$ and $np_{1/2}np_{3/2} - \omega/np_{3/2}np_{1/2} - \omega$ states acquire admixtures of the $ns_{1/2}np_j$ and $np_jns_{1/2}$ states. For reference, in these experiments the np fine-structure splitting $2\Delta \sim 2\,\mathrm{GHz}$, and the avoided crossings at ω_1 and ω_3 are up to 400 MHz for the microwave fields used.

In the absence of a dipole-dipole interaction the $ns_{1/2}ns_{1/2} + \omega$ level crosses the $np_{1/2}np_{3/2} - \omega/np_{3/2}np_{1/2} - \omega$ level at ω_{13}, but these states are coupled by the dipole-dipole couplings of the $ns_{1/2}np_j$ and $np_jns_{1/2}$ admixtures, resulting in a small, $\sim 1 - 10\,\mathrm{MHz}$, avoided crossing at ω_{13}. In Fig. 2 the size of this avoided crossing is exaggerated.

While the Floquet energy level diagram of Fig. 2 provides a good qualitative picture, to provide a more quantitative description we consider a simple model based on the interaction of two atoms, A and B, with their internuclear axis $\vec{R}$ inclined at an angle θ with respect to the z axis, the axis of quantization defined by the linearly polarized microwave field $\hat{z}E\sin\omega t$. Due to the three-dimensional nature of the dipole-dipole interaction we must take the magnetic quantum numbers into account. Accordingly, a typical field-free initial Floquet state is $|ns_{\frac{1}{2}\frac{1}{2}}ns_{\frac{1}{2}\frac{1}{2}}\rangle_{+1}$, in which both atoms have $m_j = 1/2$, and the subscript $+1$ indicates that one microwave photon has been added to the molecular state, which is a direct product of the two atomic states. There are 4 initial states and 16 final states.

In the presence of the microwave field the nominal $ns_{\frac{1}{2}\frac{1}{2}}ns_{\frac{1}{2}\frac{1}{2}} + \omega$ state has an admixture of $nsnp_j$ and np_jns states. Explicitly, it is given in perturbation theory by

$$|ns_{\frac{1}{2}\frac{1}{2}}ns_{\frac{1}{2}\frac{1}{2}}\rangle^E_{+1} = |ns_{\frac{1}{2}\frac{1}{2}}ns_{\frac{1}{2}\frac{1}{2}}\rangle_{+1} + \frac{z_3E}{2\Delta}[|np_{\frac{3}{2}\frac{1}{2}}ns_{\frac{1}{2}\frac{1}{2}}\rangle + |ns_{\frac{1}{2}\frac{1}{2}}np_{\frac{3}{2}\frac{1}{2}}\rangle] - \frac{z_1E}{2\Delta}[|np_{\frac{1}{2}\frac{1}{2}}ns_{\frac{1}{2}\frac{1}{2}}\rangle + |ns_{\frac{1}{2}\frac{1}{2}}np_{\frac{1}{2}\frac{1}{2}}\rangle]. \tag{2}$$

Similarly, in the presence of the microwave field a typical final state is given by

$$|np_{\frac{1}{2}-\frac{1}{2}}np_{\frac{3}{2}-\frac{1}{2}}\rangle^E_{-1} = |np_{\frac{1}{2}-\frac{1}{2}}np_{\frac{3}{2}-\frac{1}{2}}\rangle_{-1} + \frac{z_1E}{2\Delta}|ns_{\frac{1}{2}-\frac{1}{2}}np_{\frac{3}{2}-\frac{1}{2}}\rangle - \frac{z_3E}{2\Delta}|np_{\frac{1}{2}-\frac{1}{2}}ns_{\frac{1}{2}-\frac{1}{2}}\rangle. \tag{3}$$

In Eqs. (2) and (3), z_j is an atomic dipole matrix element. We need z_j and several other matrix elements, which we define as

$$\begin{aligned}
z_1 &= \langle ns_{\frac{1}{2}\frac{1}{2}}|z|np_{\frac{1}{2}\frac{1}{2}}\rangle = \frac{-r_n}{3},\\
z_3 &= \langle ns_{\frac{1}{2}\frac{1}{2}}|z|np_{\frac{3}{2}\frac{1}{2}}\rangle = \frac{\sqrt{2}r_n}{3},\\
x_1 &= \langle ns_{\frac{1}{2}\frac{1}{2}}|x|np_{\frac{1}{2}\frac{-1}{2}}\rangle = \frac{-r_n}{3},\\
x_3 &= \langle ns_{\frac{1}{2}\frac{1}{2}}|x|np_{\frac{3}{2}\frac{-1}{2}}\rangle = \frac{r_n}{3\sqrt{2}},\\
x_{33} &= \langle ns_{\frac{1}{2}\frac{1}{2}}|x|np_{\frac{3}{2}\frac{3}{2}}\rangle = \frac{-r_n}{\sqrt{6}},
\end{aligned} \tag{4}$$

where r_n is the radial matrix element $\langle ns|r|np\rangle$. The two levels of Eqs. (2) and (3) are coupled by the dipole-dipole interaction V_{dd}, given by

$$V_{\mathrm{dd}} = \frac{\vec{r}_A\cdot\vec{r}_B}{R^3} - \frac{3(\vec{r}_A\cdot\vec{R})(\vec{r}_B\cdot\vec{R})}{R^3}, \tag{5}$$

with $\vec{r}_A$ and $\vec{r}_B$ being the internal positions of the Rydberg electrons in atoms A and B.

Introducing the dipole-dipole interaction of Eq. (5) between the two levels of Eqs. (2) and (3) leads to the coupling matrix element

$$\Omega(\theta) = \langle ns_{\frac{1}{2}\frac{1}{2}}ns_{\frac{1}{2}\frac{1}{2}}|^E_{+1}V_{\mathrm{dd}}|np_{\frac{3}{2}-\frac{1}{2}}np_{\frac{1}{2}-\frac{1}{2}}\rangle^E_{-1} = -\frac{3E^2\sin^2\theta}{4\Delta^2R^3}\left[x_3^2z_1z_3 + x_1^2z_1z_3 + x_1x_3z_1^2 + x_1x_3z_3^2\right]. \tag{6}$$

The initial state of Eq. (6) is coupled to ten of the possible final states by matrix elements analogous to the one given in Eq. (6). The $\Delta m_j = 0$ transitions, for example, to $|np_{\frac{1}{2}\frac{1}{2}}np_{\frac{3}{2}\frac{1}{2}}\rangle^E_{-1}$, do not occur; the terms analogous to those in the square brackets of Eq. (6) cancel.

The final states are not coupled to each other, and we make the assumption that they are not coupled to another initial state. This assumption is reasonable in the present case in which much of the transition probability occurs in the perturbative regime. With this approach the Hamiltonian matrix for the ten final states coupled to the initial state of Eq. (6) can be written in the

following form. We show only five of the ten final states since the other five are the same atomic states with the two atoms interchanged, for example, $np_{\frac{1}{2}\frac{1}{2}}np_{\frac{3}{2}\frac{3}{2}}$ instead of $np_{\frac{3}{2}\frac{3}{2}}np_{\frac{1}{2}\frac{1}{2}}$. The matrix elements are unchanged. The states of the matrix are, in order, $ns_{\frac{1}{2}\frac{1}{2}}ns_{\frac{1}{2}\frac{1}{2}}$, $np_{\frac{3}{2}\frac{3}{2}}np_{\frac{1}{2}\frac{1}{2}}$, $np_{\frac{3}{2}-\frac{1}{2}}np_{\frac{1}{2}\frac{1}{2}}$, $np_{\frac{3}{2}\frac{3}{2}}np_{\frac{1}{2}-\frac{1}{2}}$, $np_{\frac{3}{2}\frac{1}{2}}np_{\frac{1}{2}-\frac{1}{2}}$, and $np_{\frac{3}{2}-\frac{1}{2}}np_{\frac{1}{2}-\frac{1}{2}}$:

$$H(\theta)=\chi\begin{pmatrix}\delta & 0.015\Theta_1 & 0.044\Theta_1 & 0.030\Theta_2 & -0.018\Theta_1 & -0.052\Theta_2 & \cdots\\ 0.015\Theta_1 & 0 & 0 & 0 & 0 & 0 & \cdots\\ 0.044\Theta_1 & 0 & 0 & 0 & 0 & 0 & \\ 0.030\Theta_2 & 0 & 0 & 0 & 0 & 0 & \\ -0.018\Theta_1 & 0 & 0 & 0 & 0 & 0 & \\ -0.052\Theta_2 & 0 & 0 & 0 & 0 & 0 & \\ \vdots & \vdots & & & & & \ddots\end{pmatrix}, \tag{7}$$

where δ is the detuning from the two-photon $ns_{1/2}ns_{1/2} - np_{1/2}np_{3/2}/np_{3/2}np_{1/2}$ resonance, $\Theta_1 = -3\sin\theta\cos\theta$, $\Theta_2 = 2-3\sin^2\theta$, and

$$\chi=\frac{E^2\langle ns|r|np\rangle^4}{4\Delta^2R^3}. \tag{8}$$

At or near resonance only two of the eigenstates of Eq. (7) contain the initial state, so the initial state is coupled to a single state, which is a linear superposition of the final basis states. The eigenvalues of the two coupled states are $\pm\Omega(\theta)$, where $\Omega(\theta)$ is the square root of the sum of the squares of the of-diagonal elements of row 1 or column 1. For the Hamiltonian of Eq. (7) $\Omega(0)$, $\Omega(\pi/4)$, and $\Omega(\pi/2)$ take the values -0.170χ, -0.114χ, and -0.085χ, respectively.

We average $\Omega(\theta)$ over θ to obtain

$$\Omega_{ns_{\frac{1}{2}\frac{1}{2}}ns_{\frac{1}{2}\frac{1}{2}}}=-0.109\chi. \tag{9}$$

The $|ns_{\frac{1}{2}-\frac{1}{2}}ns_{\frac{1}{2}-\frac{1}{2}}\rangle^E_{+1}$ state obviously has the same value of Ω.

The $ns_{\frac{1}{2}-\frac{1}{2}}ns_{\frac{1}{2}\frac{1}{2}}$ and $ns_{\frac{1}{2}\frac{1}{2}}ns_{\frac{1}{2}-\frac{1}{2}}$ states are also coupled to ten final states and have the same value of Ω. Accordingly, we set

$$\bar{\Omega}=0.109\chi. \tag{10}$$

To an excellent approximation we can represent the radial matrix element and the detuning Δ, half the np fine-structure interval with the n scalings [31]

$$\langle ns|r|np\rangle=1.10n^{*2} \tag{11}$$

and [32]

$$\Delta=0.0066n^{*-3}, \tag{12}$$

where n^* is the effective quantum number of the $np_{3/2}$ state; $n^*=n-2.65$. Introducing these scalings leads to the n^{*14} dependence of $\bar{\Omega}$. Explicitly,

$$\bar{\Omega}=\frac{\eta n^{*14}E^2}{R^3}, \tag{13}$$

where η is the numerical constant; $\eta=3.66\times10^3$. As we shall show, the transition probability at resonance is proportional to $\bar{\Omega}$ and thus to the product ρ_0E^2, where ρ_0 is the Rydberg atom density at the center of the trap.

III. EXPERIMENTAL APPROACH

As described previously, we use a vapor loaded magneto-optical trap (MOT) containing ^{85}Rb [33]. The MOT cloud is located at the center of a four-rod electrode structure used to provide a field-ionization pulse. The trapping lasers provide a steady population in the $5p_{3/2}$ state, and atoms are excited from it to an ns Rydberg state by a 480-nm laser pulse. To generate the 480-nm pulses we begin with a 960-nm single-mode diode laser. Its output is amplified by a tapered amplifier followed by two stages of pulsed dye amplification, producing 960-nm pulses ~10 ns long at a 15-Hz repetition rate. The 960-nm pulses are frequency doubled to produce 480-nm pulses with a bandwidth of 150 MHz and pulse energies of 10 μJ. The 480-nm beam is focused to a 0.15-mm-diameter (full width at half maximum, FWHM) spot where it crosses the MOT.

To detect the Rydberg atoms we field ionize them by applying a high-voltage pulse to two of the four rods. The resulting ions are driven to a microchannel plate (MCP) detector, the output of which is further amplified, with a voltage gain of 25, and sent to gated integrators.

The microwaves are generated using an Agilent E8257D frequency synthesizer. Its continuous-wave output is formed into 0.5-μs-long pulses with a General Microwave DM862B switch. The pulses are used to drive a Millitech AMC-28-3FH00 active doubler that produces an output in the 26–40 GHz range which drives either a Pacific Millimeter V2W0 passive doubler or W3W0 passive tripler to produce frequencies from 50 to 110 GHz. There is a precision attenuator after the passive multiplier followed by a waveguide and a horn. The entire microwave system is outside the vacuum chamber, and the microwaves propagate into the chamber through a 4-in.-diameter window.

The timing sequence is as follows. Atoms are excited to the ns Rydberg state by the 480-nm laser pulse. After a 20-ns delay they are exposed to a 0.5-μs microwave pulse, followed in 20 ns by a 1-μs rise-time field-ionization pulse. The amplitude of the field pulse is chosen to provide good temporal resolution of the signals from the ns and np states. The np atoms are ionized earlier, at a lower field than the ns atoms, and we detect them with a 200-ns wide gate. We detect the total field-ionization signal, from both ns and np atoms, with a 1500-ns-wide gate. Both signals are recorded in a computer for later analysis. The trap magnetic field is not turned off for the Rydberg excitation since we observe negligible difference between the resonances observed under otherwise similar conditions with and without field switching.

To compare the observed transition probabilities to a model we need to know the Rydberg atom density and the microwave field. To determine the density we have measured the diameter

(FWHM) of the MOT to be 0.65 mm using a linear array, and we assume it to have a spherical Gaussian density distribution. We have measured the 480-nm laser beam diameter (FWHM) at the MOT to be 0.15 mm using a knife edge, and we assume it to have a Gaussian intensity distribution. The Rydberg atom density is thus given by

$$\rho(x,y,z) = \rho_0 e^{-\frac{x^2+y^2+z^2}{r_M^2}} e^{-\frac{x^2+y^2}{r_L^2}}, \tag{14}$$

where $r_M = 0.47\,\text{mm}$, $r_L = 0.075\,\text{mm}$, and ρ_0 is the density at the center of the trap. It is convenient to rewrite Eq. (14) as [34]

$$\rho(x,y,z) = \rho_0 e^{-\frac{x^2+y^2}{r_T^2}} e^{-\frac{z^2}{r_M^2}}, \tag{15}$$

where $1/r_T^2 = 1/r_M^2 + 1/r_L^2$.

The number of Rydberg atoms N is obtained by integrating the density over the volume of the trap, yielding

$$N = \rho_0 \pi^{\frac{3}{2}} r_T^2 r_M. \tag{16}$$

N is proportional to the total Rydberg signal detected in the 1500-ns-wide gate, which is calibrated in the following way. We assign a quantum efficiency of 0.3 to the MCP [35]. We have measured the MCP gain to be 5×10^5, and the voltage gain of the amplifier after the MCP is 25. The sensitivities of both gated integrators are set so that a 0.1-V average input yields a 10-V output. Thus a total Rydberg signal S_{tot} of 1 V from the 1500-ns gate integrator represents 4500 Rydberg atoms and a peak density of $\rho_0 = 2.6\times10^8\ \text{cm}^{-3}$, and a 1-V signal S_{np} from the 200-ns integrator represents 600 np atoms. The average transition probability $P = \frac{S_{np}}{7.5 S_{\text{tot}}}$. We estimate the uncertainty in the number of atoms to be a factor of 3.

The other important calibration is the microwave field. The use of a precision attenuator provides an excellent relative calibration, and to put it on an absolute basis we measure the width of the nearby, ∼1 GHz away, $ns - np_{1/2}$ atomic transition as a function of attenuation. It has a width (FWHM) given by

$$\Delta\omega = 2\langle ns_{\frac{1}{2}\frac{1}{2}}|z|np_{\frac{1}{2}\frac{1}{2}}\rangle E = \tfrac{2}{3}\langle ns|r|np\rangle E. \tag{17}$$

We measured the resonance widths from a few MHz at the lowest microwave powers up to over 100 MHz to calibrate the attenuators. The microwaves are reflected to some extent by the four-rod structure and by the chamber walls, leading to an uneven frequency response. As a consequence, we estimate the field calibration to have a 20% uncertainty.

IV. OBSERVATIONS

To record the resonances we sweep the microwave frequency across the resonance over many shots of the laser while recording both the np and the total Rydberg signals. The sweeps are repeated until an acceptable signal-to-noise ratio is obtained. In Fig. 3 we show a series of resonances taken at constant density with different microwave field amplitudes. There are several features to note in these data. The resonances are asymmetric. The high-frequency side is sharp, corresponding to a half width at half maximum (HWHM) of 5 MHz, and there is an obvious wing on the low-frequency side extending ∼20 MHz. The resonance occurs at the expected frequency. The arrow in Fig. 3 at 87 525.8 GHz shows the frequency of the $36s_{1/2}36s_{1/2} - 36p_{1/2}36p_{3/2}$ transition computed using the known quantum defects of the Rb ns and np states [32]. As shown in Fig. 3, the peak of the resonance is very close to the computed frequency, which is typical of our observations. In Table II we present the observed resonance frequencies and those calculated from the known quantum defects. Typically the experimental frequency is lower due to the low-frequency wing. There is a background signal due to several sources. The separation of the ns and np field-ionization signals is not perfect. In setting the 200-ns gate our goal is to capture the entire np signal, and as a result we also capture a few percent of the ns signal. In addition, black-body radiation drives atoms from the ns to the np state. Both of these contributions are linear in the number of Rydberg atoms excited. There is also a small contribution which is quadratic in the number of Rydberg atoms excited. Such a dependence has been observed by Nascimento *et al.* who observed np states accompanying high-power 480-nm excitation of Rb ns states [36]. They attributed the production of np atoms to AC Stark shifts bringing pairs of ns atoms into Forster resonance with $np(n-1)p$ pairs. Our 480-nm powers are 2 orders of magnitude lower, and we observe no sign of power

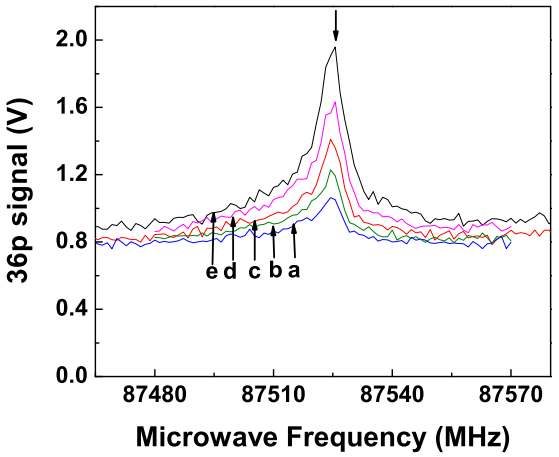

FIG. 3. Observed $36s36s \rightarrow 36p_{1/2}36p_{3/2}$ resonances at constant density and microwave field amplitudes of (a) 282, (b) 316, (c) 355, (d) 398, and (e) 447 mV/cm. The arrow indicates the calculated frequency of 87 525.8 MHz.

TABLE II. Frequencies of the $ns_{1/2}ns_{1/2} \rightarrow np_{1/2}np_{3/2}/np_{3/2}np_{1/2}$ transitions.

n	Observed frequency (MHz)	Calculated frequency (MHz)
34	105 509.5(25)	105 514.0
35	95 955.6(20)	95 960.1
36	87 524.8(20)	87 525.8
38	73 405.0(20)	73 404.9
39	67 474.7(20)	67 474.0
40	62 165.7(15)	62 165.3
41	57 396.0(20)	57 399.1
42	53 107.8(15)	53 108.0

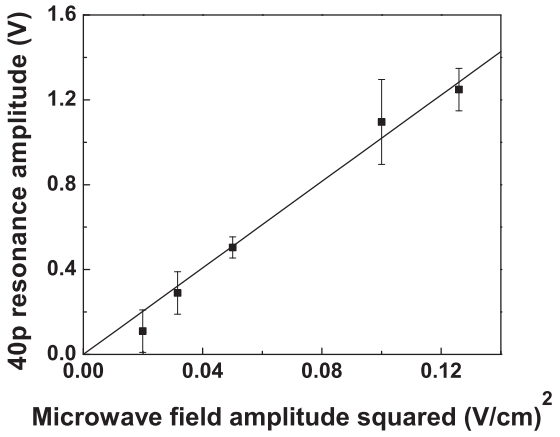

FIG. 4. The $40s_{1/2}40s_{1/2}-40p_{1/2}40p_{3/2}/40p_{3/2}40p_{1/2}$ resonance amplitude at constant density vs the microwave field squared, showing the quadratic dependence of the transition probability on the microwave field.

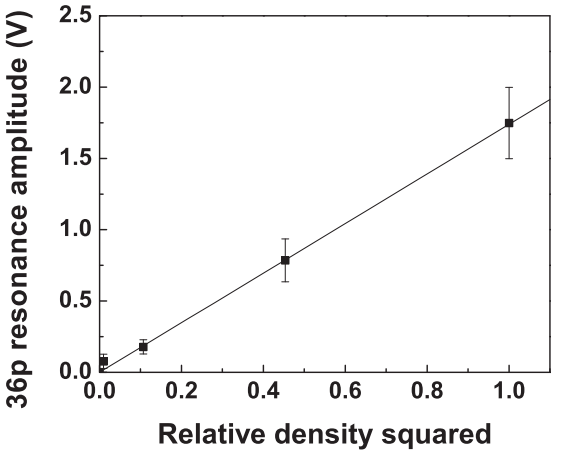

FIG. 5. Amplitude of the $38s_{1/2}38s_{1/2} \rightarrow 38p_{1/2}38p_{3/2}/38p_{3/2}38p_{1/2}$ resonance signal at a microwave field of 316 mV/cm vs the squared density at a constant microwave field amplitude.

broadening of the $5p-ns$ transition, so this process is not possible. Finally, the background increases slightly with the microwave field due to the fact that the frequency range of Fig. 3 is in the wings of the $36s-36p_j$ transitions.

The sharp increase in the resonance amplitude with increasing microwave field is not surprising, since the $ns_{1/2}ns_{1/2}-np_{1/2}np_{3/2}$ transition probability at resonance is expected to exhibit a quadratic dependence on the microwave field amplitude. To show this dependence explicitly, in Fig. 4 the resonance amplitudes of the $40s_{1/2}40s_{1/2}-40p_{1/2}40p_{3/2}$ transition at constant density are plotted vs the square of the microwave field.

We expect the transition probability to be proportional to $\rho_0 E^2$, or NE^2, and to test this notion we need to measure the density dependence of the amplitude of the resonance signal. One approach is to record series of resonances at the same microwave fields but different densities. Since the amplitude of the resonance signal is proportional to the product of the number of atoms and the transition probability, it should depend quadratically on the density, all other parameters being equal. To show the quadratic dependence most clearly, in Fig. 5 we show a plot of the amplitude of the resonance signal vs the square of the Rydberg atom density for $n=38$. As expected, it exhibits a linear dependence on the squared density. A second approach, which we have usually used, is the following. With a fixed microwave field we change the intensity of the 480-nm light with a neutral density filter wheel to provide a continuous change in the number of Rydberg atoms. As the wheel is slowly rotated over many shots of the laser, we record both the np and total Rydberg atom signals for the microwave frequency tuned to the resonance and detuned by $\sim 40-200$ MHz. An example of filter wheel scans is shown in Fig. 6, which is a plot of the on-resonant and of-resonant signals vs the total signal for the $38s_{1/2}38s_{1/2}-38p_{1/2}38p_{3/2}/38p_{3/2}38p_{1/2}$ transition. The difference between the two curves is the resonant np signal S_{np} as a function of the total signal $S_{\rm tot}$. From each wheel scan we construct the average transition probability $P=S_{np}/(7.5S_{\rm tot})$, and we convert $S_{\rm tot}$ into ρ_0, the density at the center of the trap. In Fig. 7 we plot $P/(n^{*14}\rho_0 E^2)$ vs n. We expect $P/(n^{*14}\rho_0 E^2)$ to be a constant. Although there is substantial scatter, which we attribute primarily to the uncertainty in the microwave field calibration, the data are certainly consistent with an n-independent value of 4.0×10^{-31} cm^3 (V/cm)$^{-2}$, as shown by the broken line.

V. DISCUSSION

The data of the previous section allow a comparison of the magnitudes of the observed signals to those expected from the Forster Floquet model. Using $\bar{\Omega}$ of Eq. (13) we can calculate the transition probability at resonance. If there are two states coupled by $\bar{\Omega}$, the population oscillates between the initial and final states at angular frequency $2\bar{\Omega}$. If the microwave pulse has duration T, at the end of the pulse the transition probability at resonance $P(R)$ for a pair of atoms spaced by

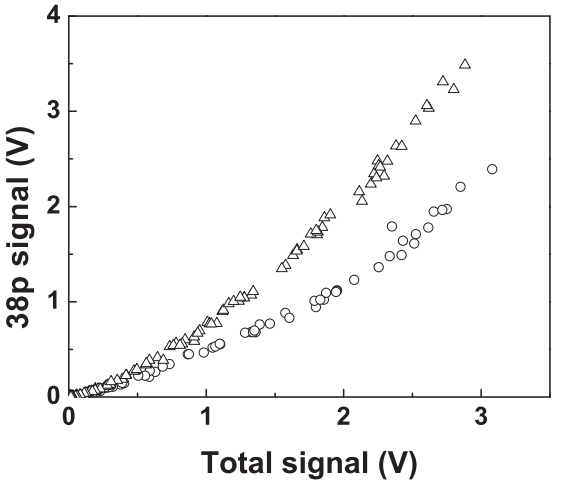

FIG. 6. The on-resonant (△) and of-resonant (○) $38p$ signals at a microwave field of 199 mV/cm vs the total number of Rydberg atoms. The difference between the two sets of data is the resonant signal vs the total number of Rydberg atoms.

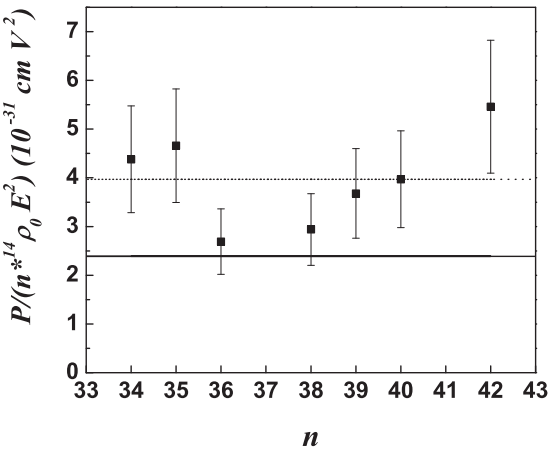

FIG. 7. Plot of $P/n^{*14}\rho_0 E^2$ vs n, showing the n^{*14} dependence of the transition probability. The average of the experimental points, 4.0×10^{-31} cm V^2, is shown by the broken line. The value calculated from Eq. (30) is shown by the solid line.

R is given by

$$P(R) = \sin^2 \bar{\Omega} T. \tag{18}$$

For a given microwave field E we define the internuclear spacing R_T using

$$\bar{\Omega} T = \frac{\eta n^{*14} E^2 T}{R_T^3 \gamma} = \frac{\pi}{2}. \tag{19}$$

In Eq. (19) we have introduced the phenomenalogical constant γ to account for the fact that the observed resonances are broader than the transform limit of the microwave-pulse length. There are more elegant ways of introducing the broadening, as shown by Yakshina *et al.* [21], but the result is the same.

It is useful to recast Eq. (19) as

$$R_T^3 = \frac{2\eta n^{*14} E^2 T}{\pi \gamma}. \tag{20}$$

With our 0.5 $-\mu$s-long microwave pulse we expect to observe resonances with a FWHM = 1 MHz, but we do not observe such narrow resonances. The typical half width on the high-frequency side is 5 MHz, five times larger than expected. To account for this broadening, we set $\gamma = 5$. Pairs spaced by $R < R_T$ oscillate back and forth between the initial state and the final state, with an average transition probability of 1/2. Pairs separated by $R \geqslant R_T$ have a transition probability given by Eq. (18), which we approximate by

$$P(R) = \bar{\Omega}^2 T^2. \tag{21}$$

At a Rydberg density ρ we define the average spacing $R_{\rm av}$ by

$$\frac{1}{\rho} = \frac{4\pi R_{\rm av}^3}{3}, \tag{22}$$

and the probability of an atom having its nearest neighbor a distance R away is given approximately by

$$\frac{dN}{dR} = \begin{cases} \frac{3R^2}{R_{av}^3}, & R \leqslant R_{\rm av}, \\ 0, & R > R_{\rm av}. \end{cases} \tag{23}$$

The average resonant transition probability for density ρ is computed using a transition probability of 1/2 for $R \leqslant R_T$ and Eq. (18) for $R > R_T$, resulting in

$$P(\rho) = \frac{1}{2}\frac{R_T^3}{R_{\rm av}^3} + \int_{R_T}^{R_{\rm av}} \left(\frac{\eta n^{*14} E^2}{R^3 \gamma}\right)^2 \frac{T^2 3R^2 {\rm d}R}{R_{\rm av}^3}. \tag{24}$$

Assuming $R_T^3 \ll R_{\rm ac}^3$, we can let the upper limit of the integral go to infinity, in which case

$$P(\rho) = \frac{1}{2}\frac{R_T^3}{R_{\rm av}^3} + \left(\frac{\pi}{2}\right)^2 \frac{R_T^3}{R_{\rm av}^3}. \tag{25}$$

To a good approximation

$$P(\rho) = \frac{3R_T^3}{R_{\rm av}^3} = \frac{8\eta n^{*14} E^2 T \rho}{\gamma}. \tag{26}$$

Averaging this transition probability over density yields the average transition probability

$$P = \int_0^{\rho_0} \frac{dN}{d\rho} P(\rho) d\rho. \tag{27}$$

For the density distribution of Eq. (15), $dN/d\rho$ takes the form [34]

$$\frac{dN}{d\rho} = \pi r_T^2 r_M [ln(\rho_0/\rho)]^{1/2}, \tag{28}$$

and the integral of Eq. (27) yields

$$P = 0.35 P(\rho_0) = \frac{2.8\eta n^{*14} \rho_0 E^2 T}{\gamma}. \tag{29}$$

With $T = 0.5$ μs, $\eta = 3.7\times10^3$, and $\gamma = 5$, we can rewrite Eq. (29) in laboratory units as

$$P = 2.4\times10^{-31} n^{*14} \rho_0 E^2, \tag{30}$$

where ρ_0 is expressed in cm^{-3} and E in V/cm. In Fig. 7 we show the calculated value of $P/n^{*14}\rho_0 E^2$ as the solid line. It is 2/3 the experimental value, well within our density measurement uncertainty.

An initially surprising aspect of the resonances was their asymmetry. As shown by Fig. 3 the resonances have low-frequency wings. With these particular atomic states a low-frequency wing could be the result of a Stark shift from a stray electric field. Possible sources of stray fields are ions, accidental bias voltages on the rods, and the MCP. Two observations suggest that stray fields are not important. First, we see a negligible number of ions. Second, and more important, in doing the microwave attenuator calibration we see no evidence of Stark shifts or broadening of the $ns - np_{1/2}$ transitions, even at the lowest microwave powers, where the resonances are 2–3 MHz wide.

We attribute the wings to the van der Waals interaction of the $np_{1/2}np_{3/2}/np_{3/2}np_{1/2}$ states with the nearby $ns_{1/2}(n+1)s_{1/2}$ state. For atoms spaced by the characteristic spacing of atoms in the trap this van der Waals interaction is negligible, ~10 kHz, and for this reason, we initially discounted it. However, for the few percent of the atoms which undergo the transition, the characteristic spacing is much smaller, $\sim R_T$, leading to an observable van der Waals shift.

We can estimate the van der Waals shift starting from Eqs. (26) and (29). If we assume a transition probability of

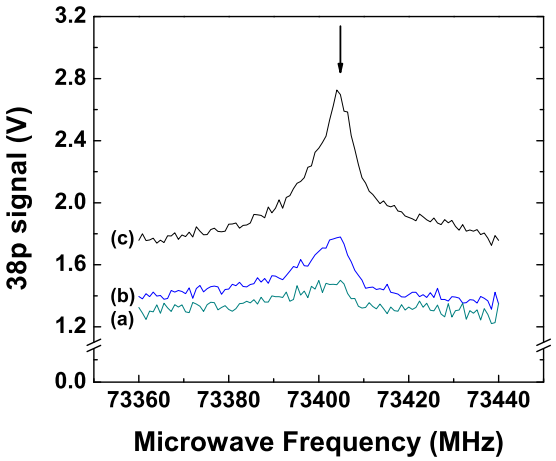

FIG. 8. The $38s_{1/2}38s_{1/2}-38p_{1/2}38p_{3/2}/38p_{3/2}38p_{1/2}$ resonance observed at constant density and microwave fields of (a) 141, (b) 177, and (c) 251 mV/cm. At low field the transition can only occur for closely spaced atoms, leading to a resonance dominated by the van der Waals shift. As the microwave field is raised, atoms separated by larger distances, with smaller van der Waals shifts, undergo the transition, leading to a much sharper peak at the calculated frequency of 73 404.9 MHz, as shown by the arrow.

3%, $R_T^3 = 0.03R_{\mathrm{av},0}^3$, where $R_{\mathrm{av},0}$ is the average spacing at the center of the trap, the van der Waals shift is almost 3 orders of magnitude larger than for a pair of atoms at the trap's characteristic spacing of R_{av}. If we use $n = 39$ as an example, the dipole-dipole coupling between the $39p_{1/2}39p_{3/2}$ and $39s_{1/2}40s_{1/2}$ states is approximately given by

$$V_{\mathrm{dd}} = \frac{\langle 39p|r|39s\rangle\langle 39p|r|40s\rangle}{R_T^3}. \tag{31}$$

For a 3% transition probability at the maximum trap density the resulting dipole-dipole coupling is 78 MHz, leading to a 3-MHz van der Waals shift. The shifts implicit in the low-frequency wings are larger than this estimate, but we have not taken into account the atoms closer together than R_T.

The line shape has a definite microwave field dependence. At low microwave fields the low-frequency wing is more pronounced, which can be seen in the set of resonances shown in Fig. 4. This property is more apparent in Fig. 8, a set of $38s_{1/2}38s_{1/2} - 38p_{1/2}38p_{3/2}/38p_{3/2}38p_{1/2}$ resonances taken at a constant density and three different microwave fields. At low microwave field there is not a prominent peak at the unshifted $38s_{1/2}38s_{1/2} - 38p_{1/2}38p_{3/2}/38p_{3/2}38p_{1/2}$ frequency. However, as the microwave field is raised, a pronounced peak appears at the unshifted $38s_{1/2}38s_{1/2} - 38p_{1/2}38p_{3/2}$ frequency. This development is consistent with our expectation based on the coupling given by Eq. (13). If the atomic density is fixed, as in Fig. 8, since R_T^3 has a quadratic dependence on the microwave field, increasing E increases R_T^3, rapidly reducing the van der Waals shift, which in turn leads to a sharp feature at the $38s_{1/2}38s_{1/2} - 38p_{1/2}38p_{3/2}/38p_{3/2}38p_{1/2}$ frequency.

VI. CONCLUSION

We have presented a systematic study of the process Rb $ns_{1/2}$ + Rb $ns_{1/2} + 2\hbar\omega \rightarrow$ Rb $np_{1/2}$ + Rb $np_{3/2}$. It is a process which depends critically on the three-dimensional nature of the dipole-dipole interaction. In addition, the n^{14} dependence of the transition probability is, to our knowledge, the highest of any two-body process. Processes involving more than two atoms can, of course, have a higher n dependence. Finally, these measurements underscore the fact that when the observed signal is due only to the few most closely spaced atoms, interactions such as the van der Waals interaction, which are negligible for most of the atoms in the trap, become important.

ACKNOWLEDGMENTS

It is a pleasure to acknowledge helpful discussions with R. R. Jones and P. Pillet and the support of the Air Force Office of Scientific Research under Grant No. FA9550-14-1-0288. J.N. was supported by the Thailand Center of Excellence in Physics (Grant No. ThEP-61-PHY-MU3). R.A. would like to acknowledge HEC, Pakistan, for their support under PPCR funding.

[1] M. D. Lukin, M. Fleischhauer, R. Cote, L. M. Duan, D. Jaksch, J. I. Cirac, and P. Zoller, Phys. Rev. Lett. **87**, 037901 (2001).
[2] D. Moller, L. B. Madsen, and K. Molmer, Phys. Rev. Lett. **100**, 170504 (2008).
[3] M. Saffman, T. G. Walker, and K. Molmer, Rev. Mod. Phys. **82**, 2313 (2010).
[4] I. I. Beterov, M. Saffman, E. A. Yakshina, D. B. Tretyakov, V. M. Entin, S. Bergamini, E. A. Kuznetsova, and I. I. Ryabtsev, Phys. Rev. A **94**, 062307 (2016).
[5] S. Wuster, C. Ates, A. Eisfeld, and J. M. Rost, Phys. Rev. Lett. **105**, 053004 (2010).
[6] T. Scholak, T. Wellens, and A. Buchleitner, Phys. Rev. A **90**, 063415 (2014).
[7] D. Barredo, H. Labuhn, S. Ravets, T. Lahaye, A. Browaeys, and C. S. Adams, Phys. Rev. Lett. **114**, 113002 (2015).
[8] H. Bernien, S. Schwartz, A. Keesling, H. Levine, A. Omran, H. Pichler, S. Choi, A. S. Zibrov, M. Endres, M. Greiner, V. Vuletic, and M. D. Lukin, Nature (London) **534**, 667 (2016).
[9] P. Schauss, M. Cheneau, M. Endres, T. Fukahara, S. Hild, A. Omran, T. Pohl, C. Gross, S. Kuhr, and I. Bloch, Nature (London) **491**, 87 (2012).
[10] E. Urban, T. A. Johnson, T. Henage, L. Isenhower, D. D. Yavuz, T. G. Walker, and M. Saffman, Nat. Phys. **5**, 110 (2009).
[11] A. Gaëtan, Y. Miroshnychenko, T. Wilk, A. Chotia, M. Viteau, D. Comparat, P. Pillet, A. Browaeys, and P. Grangier, Nat. Phys. **5**, 115 (2009).
[12] S. Baur, D. Tiarks, G. Rempe, and S. Durr, Phys. Rev. Lett. **112**, 073901 (2014).
[13] W. R. Anderson, J. R. Veale, and T. F. Gallagher, Phys. Rev. Lett. **80**, 249 (1998).

[14] I. Mourachko, D. Comparat, F. de Tomasi, A. Fioretti, P. Nosbaum, V. Akulin, and P. Pillet, Phys. Rev. Lett. **80**, 253 (1998).
[15] T. J. Carroll, K. Claringbould, A. Goodsell, M. J. Lim, and M. W. Noel, Phys. Rev. Lett. **93**, 153001 (2004).
[16] M. R. Kutteruf and R. R. Jones, Phys. Rev. Lett. **108**, 013001 (2012).
[17] P. Bohlouli-Zanjani, J. A. Petrus, and J. D. D. Martin, Phys. Rev. Lett. **98**, 203005 (2007).
[18] A. Tauschinsky, C. S. E. van Ditzhuijzen, L. D. Noordam, and H. B. van Linden van den Heuvell, Phys. Rev. A **78**, 063409 (2008).
[19] C. S. E. van Ditzhuijzen, A. Tauschinsky, and H. B. van Linden van den Heuvell, Phys. Rev. A **80**, 063407 (2009).
[20] D. B. Tretyakov, V. M. Entin, E. A. Yakshina, I. I. Beterov, C. Andreeva, and I. I. Ryabtsev, Phys. Rev. A **90**, 041403(R) (2014).
[21] E. A. Yakshina, D. B. Tretyakov, I. I. Beterov, V. M. Entin, C. Andreeva, A. Cinins, A. Markovski, Z. Iftikhar, A. Ekers, and I. I. Ryabtsev, Phys. Rev. A **94**, 043417 (2016).
[22] Y. Yu, H. Park, and T. F. Gallagher, Phys. Rev. Lett. **111**, 173001 (2013).
[23] J. Lee, J. Iqbal, and T. F. Gallagher, Phys. Rev. A **96**, 012507 (2017).
[24] F. Varsanyi and G. H. Dieke, Phys. Rev. Lett. **7**, 442 (1961).
[25] C. Hettich, C. Schmitt, J. Zitzmann, S. Kuhn, I. Gerhardt, and V. Sandoghar, Science **298**, 385 (2002).
[26] R. W. Falcone, W. R. Green, J. C. White, J. F. Young, and S. E. Harris, Phys. Rev. A **15**, 1333 (1977).
[27] P. Pillet, R. Kachru, N. H. Tran, W. W. Smith, and T. F. Gallagher, Phys. Rev. A **36**, 1132 (1987).
[28] J. Lee, P. Kongkhambut, and T. F. Gallagher, Phys. Rev. A **96**, 061401(R) (2017).
[29] E. Pedrozo-Penafiel, R. R. Paiva, F. J. Vivanco, V. S. Bagnato, and K. M. Farias, Phys. Rev. Lett. **108**, 253004 (2012).
[30] J. H. Shirley, Phys. Rev. **138**, B979 (1965).
[31] T. G. Walker and M. Saffman, Phys. Rev. A **77**, 032723 (2008).
[32] W. Li, I. Mourachko, M. W. Noel, and T. F. Gallagher, Phys. Rev. A **67**, 052502 (2003).
[33] C. Monroe, W. Swann, H. Robinson, and C. Wieman, Phys. Rev. Lett. **65**, 1571 (1990).
[34] H. Park, P. J. Tanner, B. J. Claessens, E. S. Shuman, and T. F. Gallagher, Phys. Rev. A **84**, 022704 (2011).
[35] T. Koizuma and Y. Chihara, J. Phys.: Conf. Ser. **163**, 012114 (2009).
[36] V. A. Nascimento, L. L. Caliri, A. Schwettmann, J. P. Shaffer, and L. G. Marcassa, Phys. Rev. Lett. **102**, 213201 (2009).